Ion-Beam-Induced Surface Instability of Glassy $Fe_{40}Ni_{40}B_{20}$

A. Gutzmann, S. Klaumünzer, and P. Meier
Bereich Festkörperphysik, Hahn-Meitner-Institut, POB. 390128, D-14109 Berlin, Germany
(Received 26 October 1994; revised manuscript received 27 January 1995)

Depending on the angle of incidence θ, implantation of fast heavy ions into amorphous $Fe_{40}Ni_{40}B_{20}$ leads to drastic surface smoothing ($\theta \leq 15°$) or surface roughening ($\theta \geq 20°$) when fluences between 10^{14} and 10^{15} ions/cm^2 are applied. Both effects proceed without detectable mass loss. Prior to roughening, rather regular undulations appear with wavelengths between 20 and 30 μm. It is argued that the observed surface instability is a consequence of an ion-induced shear flow which presumably occurs in all amorphous materials.

PACS numbers: 61.80.Jh, 61.43.Dq, 62.20.Dc, 68.35.Bs

Modification of a solid with an ion beam involves the modification of at least one of the surfaces of the solid. Since various physical mechanisms can contribute to surface modification, the latter can be rather complex, depending on the properties of the incident ion as well as the solid. At high kinetic ion energies E and sufficiently low irradiation temperatures T_i the projectiles are deeply implanted into the bulk and both the implanted species and generated defects do not reach the surface. In this case the main route of surface modification is believed to be surface erosion. For $E \gtrsim 1$ MeV/u, the electronic energy loss S_e of heavy ions is very large (>10 keV/nm) and creates a large number of electronically excited and/or ionized target atoms. In insulators, badly conducting semiconductors and isletlike metal film surface erosion by S_e can result in several thousand eroded surface atoms per incident ion [1–4]. However, in bulk metals and alloys, surface erosion by S_e seems to be absent and only erosion by elastic collisions between the projectiles and near surface atoms contribute (collisional sputtering) [1–4]. Thus, for heavy ions with $E \gtrsim 1$ MeV/u, the number of sputtered atoms per incident ion is less than 1 [1,2]; i.e., at a fluence of 10^{15} ions/cm^2, typically less than 1 monolayer (ML) is eroded, which is a negligible effect for most cases.

On the other hand, when a fast ion sets a large number of near-surface atoms into motion, surface modifications without detectable mass loss may result. In fact, it is now well established that in bulk amorphous metals the electronic energy loss induces transiently a large number of very mobile atoms, even at $T_i < 50$ K [5,6]. In thin samples, i.e., when the specimen thickness d is much less than the projected range R_p of the projectiles, this large mobility gives rise to a macroscopically visible growth of the sample dimensions perpendicular to the beam. The mass density remains virtually constant [5]. It is the purpose of this Letter to show that this transient mobility of atoms in amorphous metals also gives rise to drastic surface modifications in the fluence range between 10^{14} and 10^{15} ions/cm^2. These high fluences are now routinely accessible for systematic investigations because of the dedication of large ion accelerators to solid-state physics and because of a continuous improvement of the ion-source technology.

Previous studies [5,6] of the growth behavior of metallic glasses were hampered by the formation of wrinkles which ultimately destroyed a well defined irradiation geometry (cf. Fig. 3 in Ref. [5]). In order to extend significantly the fluence range and to avoid wrinkling the thick ($d > R_p$) $Fe_{40}Ni_{40}B_{20}$ samples of this work were glued with epoxy resin onto 2 mm thick copper plates. The specimen pieces (approximately 7×7 mm^2) were cut from a melt-spun glassy ribbon. The copper plates were mounted on a variable-temperature cryostat which allowed tilt angles $0 \leq \theta \leq 90°$ between the sample surface normal and the beam. The irradiations were performed at the ISL Accelerator in Berlin at $T_i = 80$ and 300 K using various beams and energies (^{127}I, $E = 1.65$ MeV/u, $R_p = 10$ μm; ^{129}Xe, $E = 1.34$ MeV/u, $R_p = 8.7$ μm; and ^{129}Xe, $E = 2.64$ MeV/u, $R_p = 13$ μm [7]). The ion fluxes Φ were kept below 2×10^{10} ions/cm^2 s, so that beam heating was negligible. Lateral uniformity of the irradiation was achieved by carefully sweeping the beam across an aperture of 5×5 mm^2. A second collimator with a circular bore of 1 to 2 mm diameter defined the irradiation spot. Prior to and after irradiation the sample surfaces were examined *ex situ* at room temperature by optical and scanning electron microscopy. A two-dimensional height profile $h(x,y)$ of each sample surface was determined by means of a computerized laser profilometer (UBM 16, UBM Messtechnik) with a lateral resolution of 1 μm and a step height resolution of $dh \approx 20$ nm. This profilometer allowed us to scan a sample area of 1 mm^2 within 18 h and to collect 10^6 data points $h(x,y)$. From these data we derived the probability density function $p(h)$ with $\int p(h)\,dh = 1$, the average height $\langle h \rangle = \int h p(h)\,dh$, and the roughness parameter R, which is given by $R^2 = \int (h - \langle h \rangle)^2\, p(h)\,dh$.

The as-quenched $Fe_{40}Ni_{40}B_{20}$ ribbon had a thickness $d = 40$ μm, $R = 1.1$ μm, and exhibited a very broad height distribution extending up to $\Delta h = h - \langle h \rangle = \pm 10$ μm (cf. inset of Fig. 1). This broad height distribution is a consequence of the melt-spinning process, because gaseous inclusions between the rotating wheel

 0031-9007/95/74(12)/2256(4)$06.00

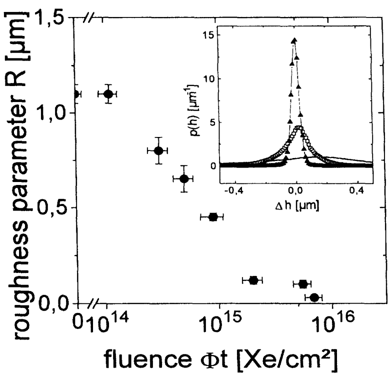

FIG. 1. Roughness parameter R_q of glassy $Fe_{40}Ni_{40}B_{20}$ irradiated with 1.3 MeV/u ^{129}Xe ions at 300 K and $\theta = 0$ as a function of the ion fluence Φt. The inset displays the height probability function $p(h)$ at $\Phi t = 0$ (solid line), $\Phi t = 2 \times 10^{15}$ Xe ions/cm^2 (open square), and $\Phi t = 6.9 \times 10^{15}$ Xe ions/cm^2 (solid triangle).

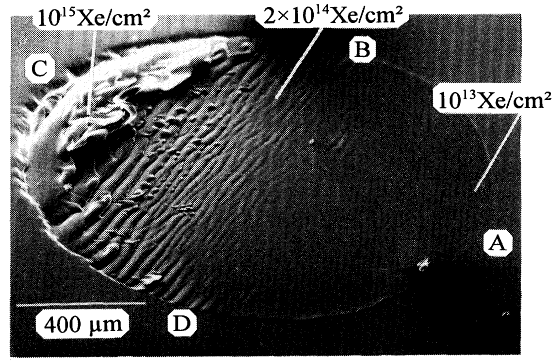

FIG. 2. This scanning electron micrograph illustrates the various stages of the surface modification during Xe implantation ($E = 2.64$ MeV/u, $T_i = 80$ K, $\theta = 45°$) into an originally polished sample. The fluence variation from the left to the right is also indicated. This sample was prepared only for illustration. The fluence values given in the text were derived from uniformly irradiated specimens. The coordinate system is x axis along line $CA \equiv$ the projection of the beam onto the plane surface, y axis along DB, z axis normal of the plane surface. The tilt angle θ is subtended by the beam axis and the z axis.

and the solidifying melt produce rather rough surfaces [8]. The material was used in the as-received state for normal-incidence experiments ($\theta = 0$). For most of the titled-target experiments the ribbon material was polished with diamond paste (0.25 μm finish) before irradiation to a final thickness $d = 30$ μm, and $R < 20$ nm.

In Fig. 1 the roughness parameter R of as-quenched $Fe_{40}Ni_{40}B_{20}$ irradiated with 1.34 MeV/u Xe ions at 300 K and $\theta = 0$ is plotted versus fluence Φt. Between 10^{14} and 2×10^{15} Xe ions/cm^2, R decreases by an order of magnitude. For $T_i = 80$ K, a rather similar curve is obtained except that the Φt scale is shifted to smaller fluences by about a factor of 5. The average heights inside and outside the bombarded region are equal. Consequently, the surface smoothing proceeds without detectable mass loss. Obviously, the grooves or "valleys" of the surface are filled up at the expense of the hills which decrease in height. This behavior is illustrated in the inset of Fig. 1, where the probability density $p(h)$ is plotted versus Δh for various fluences. As can be seen, the deeper a valley or the larger a hill the more rapidly the smoothing proceeds. At present, the final state of the smoothing process is not yet fully established. At $\Phi t = 7 \times 10^{15}$ Xe ions/cm^2 for $T_i = 300$ K, the roughness parameter reaches the experimental resolution of the laser profilometer. A first examination of smaller sample areas with a scanning tunneling microscope provides evidence that R may approach 1 nm.

When the angle θ is changed from zero to $\theta \geq 20°$, rough surfaces become again smooth on a very small length scale (≈ 1 μm). But, additionally, regular undulations start to appear at about 10^{14} ions/cm^2 ($T_i = 80$ K) with wave vectors $\mathbf{q} = (q_x, 0, 0)$ (cf. Fig. 2). If the scratches of the polishing structure have favorite wave vectors $\mathbf{q}_{\text{polish}} \approx \mathbf{q}$, then there exists an intermediate fluence range between 10^{14} and 3×10^{14} Xe ions/cm^2 ($T_i = 80$ K) where a transient enhancement of the polishing structure occurs. But at about 3×10^{14} Xe ions/cm^2 all wave vectors are locked to $\mathbf{q}$. The wavelengths lie in a narrow band ranging from 20 to 30 μm with the center at about 25 μm (Fig. 2). The wavelengths are independent of the investigated ion species and energies, independent of θ, T_i, and the starting surface topography, i.e., the same wavelength band appears on polished or as-quenched specimens. Between 10^{14} and 4×10^{14} ions/cm^2 the amplitudes grow approximately exponentially with Φt. The wavy structure starts to transform into a very complex one at 5×10^{14} ions/cm^2. At $\Phi t = 10^{15}$ ions/cm^2 ($T_i = 80$ K), the whole irradiation spot is extremely rough (Fig. 2) with amplitude spikes larger than 50 μm and the laser profilometer fails. As in the case of $\theta = 0$, the formation of the wavy structure as well as the transformation into a chaotic one proceeds without detectable mass loss.

At the borderline between the irradiated and the unirradiated material, additional features appear as soon as $\theta > 0$. Along the line DAB (cf. Fig. 2), matter is squeezed into the unirradiated region forming a damlike structure with maximum height at point A. Along the line BCD a valley forms with maximum depth and width at point C. At a fluence of $\Phi t = 10^{15}$ Xe ions/cm^2 ($E = 2.64$ MeV, $T_i = 80$ K, $\theta = 45°$) the width of the valley at point C is about 120 μm. Sometimes two or three smaller dams or valleys form. The formation of this borderline structures becomes detectable already at fluences at about 10^{13} Xe ions/cm^2 ($T_i = 80$ K).

It is clear from these experiments that, independent of θ, the bombardment of glassy $Fe_{40}Ni_{40}B_{20}$ with fast heavy ions induces drastic rearrangements of the near-surface atoms. The absence of significant mass loss rules out important contributions from surface erosion. This result is in accordance with previous findings [1–4]. Moreover, both the dependence of the wave amplitude on Φt and the orientation of $\mathbf{q}$ along the projection of the incident beam distinguish the pattern formation of this work clearly from the ripple formation occurring on amorphous materials during low-energy ion implantation [9,10]. Obviously, the passage of each fast heavy ion generates a large transient mobility of the near-surface atoms on an energy scale which, at least for the overwhelming fraction of atoms, is below the surface binding energy. It is quite suggestive that this mobility arises from just that mechanism, which produces also the mobility in the bulk resulting ultimately in the dimensional changes in thin amorphous materials [5,6]. Indeed, the exponential increase of the relative amplitude a/a_0 by a factor of 10 at $T_i = 80$ K within a fluence increment of 2×10^{14} Xe ions/cm^2 corresponds to a deformation yield $A_0 = (\Delta\Phi t)^{-1} \ln(a/a_0) = 1.2 \times 10^{-14}$ cm^2, which is exactly the low-temperature value of the deformation rate of bulk $Fe_{40}Ni_{40}B_{20}$ when mechanical constraints are absent [5]. This is not very surprising, since, with increasing a, the wave crests become essentially free of stresses and deform like the thin $Fe_{40}Ni_{40}B_{20}$ samples of the previous experiments [5,6]. Once the wave crests have formed they start to grow due to the same mechanism as in the bulk. The transition to complexity at large amplitudes is caused by the formation of wrinkles in the originally coherently aligned wave crests in the same way as wrinkles do form in thin specimens clamped partly into a sample holder [5].

Why do the undulations form? There is a growing number of recent experiments [6,11–17] which suggest that amorphous materials behave viscoelastically during fast heavy ion bombardment. It can be shown [18] that the constitutive equation

$$\frac{d\hat{\epsilon}}{dt} = \frac{1}{2G}\frac{d}{dt}\left[\hat{\sigma} - \frac{\nu}{\nu+1}(\mathrm{Tr}\hat{\sigma})\hat{I}\right] + \hat{A}_0\Phi + k_0\Phi\left[\hat{\sigma} - \frac{1}{3}(\mathrm{Tr}\hat{\sigma})\hat{I}\right] \quad (1)$$

accounts well for those experiments. In Eq. (1) $\hat{\epsilon}$, $\hat{\sigma}$, and $\hat{I}$ denote the tensors of strain, stress, and unity, respectively. $\mathrm{Tr}\hat{\sigma}$ means the trace of $\hat{\sigma}$. In the absence of irradiation $\Phi = 0$, Eq. (1) reduces to an elastic solid with shear modulus G and Poisson number ν. In the absence of stress $\hat{\sigma} = 0$, the strain rate $d\hat{\epsilon}/dt$ equals $\hat{A}_0\Phi$, which describes the growth effect of thin amorphous materials during ion bombardment [5,6] and reads [19]

$$\hat{A}_0\Phi = A_0\Phi\begin{pmatrix} 1 - 3\sin^2\theta & 0 & 3\sin\theta\cos\theta \\ 0 & 1 & 0 \\ 3\sin\theta\cos\theta & 0 & 1 - 3\cos^2\theta \end{pmatrix} \quad (2)$$

if changes of mass density are zero. A_0 depends on S_e, T_i, and the investigated material [19]. The viscous behavior at constant mass density of the glassy matter is described by the third term in Eq. (1); $(2k_0\Phi)^{-1}$ corresponds to an effective shear viscosity [20]. It should be added that the phenomenological equation (1) is the simplest way to combine elasticity, ion-beam-induced growth, and radiation-induced viscosity. For the special case $\theta = 0$, the scalar variant of Eq. (1) has been used recently to explain the ion-induced plastic flow of SiO_2 on Si [15].

If $A_0 \neq 0$ in Eq. (1), irradiation of a thick glass, originally stress-free, produces a strain which, in turn, gives rise to a stress due to the constraints supplied by the unbombarded material. For $\theta = 0$, there exists a solution of Eq. (1) with compressive stresses $\sigma_{xx} = \sigma_{yy} < 0$ and $\sigma_{xz} = \sigma_{zz} = 0$, so that $d\hat{\epsilon}/dt = d\hat{\sigma}/dt = 0$; i.e., on a perfectly planar surface with $\theta = 0$, the ion-induced net motion of atoms ceases and there is a balance between the growth strain rate and the strain relaxation by viscous flow. For a planar surface with $0 < \theta < 90°$, however, the nonvanishing off-diagonal elements in Eq. (2) and $\sigma_{xz} = 0$ at the free surface imply a nonvanishing shear flow

$$\frac{d\epsilon_{xz}}{dt} = \frac{1}{2}\left(\frac{\delta v_x}{\delta z} + \frac{\delta v_z}{\delta x}\right) = 3A_0\Phi\sin\theta\cos\theta \quad (3)$$

of the near-surface layers even in a thick target. It is clear that a rough surface with a varying θ is unstable with respect to this shear flow and that the latter provides an efficient way for surface smoothing. The magnitude of this effect is directly related to the quantity $A_0\Phi t$. Because A_0 decreases for $Fe_{40}Ni_{40}B_{20}$ by a factor of 5 when going from $T_i = 80$ to 300 K [11] this decrease can be compensated by a correspondingly higher fluence to reach the same level of surface smoothing. The shear flow also accounts for the formation of the mounds and valleys at the borderline between irradiated and unirradiated material. For example, at point C (Fig. 2) the width Δx of the valley is, according to Eq. (3),

$$\Delta x = v_x t = 6\Phi t \sin\theta\cos\theta \int_{-R_p^*\cos\theta}^{0} A_0(z)\,dz \approx 3\Phi t R_p^* A_0(z=0)\sin\theta\cos\theta,$$

where we assumed $v_z = 0$ and a linear relationship between $A_0(z)$ and z [21]. With $\Phi t = 10^{15}$ Xe ions/cm^2, $A_0(z=0) = 1.2 \times 10^{-14}$ cm^2 [5], $R_p^* \approx 10$ μm, and $\theta = 45°$ we obtain $\Delta x = 130$ μm, which is in good agreement with the measured value. At point A, however, the unirradiated sample part represents an almost rigid obstacle, i.e., $v_x = 0$. Then Eq. (3) demands $v_z \neq 0$, i.e., the glassy material flows out of the plane $z = 0$ and forms the mound. The transitions from mound to valley occur at points B and D, respectively, where the borderline between irradiated and unirradiated material runs parallel to v_x.

Equation (1) provides the starting point to formulate the equation of motion of the viscous flow of glasses subject to bombardment with fast heavy ions. The solution of the unperturbed plane shear flow is given by Eq. (3) together with normal stresses σ_{xx} and σ_{yy}, which are only equal for $\theta = 0$. These normal stresses may drive a mechanism for instability of this plane shear flow in analogy to a viscoelastic fluid flowing down a vertical plane, where long waves are predicted even at zero Reynolds number [22]. Thus a stability analysis of the equation of motion should yield the wavelengths band, its independence of θ and T_i, and the critical angle $15° < \theta < 20°$, which separates the region of mere surface smoothing from the region of undulation formation and complex roughening. This task remains to be done.

Equation (1) is very general and previous experiments [5,23] suggest that A_0 is different from zero in all amorphous materials provided the electronic energy loss is sufficiently high. Therefore, we expect that the surface instabilities reported in this Letter occur in all amorphous materials subjected to bombardment with fast heavy ions. From a microscopic point of view the quantities A_0 and k_0 stem from the same atomic mobility in the ion's wake. Recent theoretical work [24], which assumes a liquidlike state in the wake, offers a first approach to derive both A_0 and k_0 from material parameters. In this model the decisive difference between amorphous and crystalline materials results from recrystallization effects during the cooling of the liquidlike state. They are absent in glasses but render $A_0 \approx 0$ when ideal epitaxy prevails.

We thank G. Wilhelm and M. Lenzner for their technical assistance with the scanning electron microscope during the work, and P. Bauer (University of Erlangen) for making available his atomic force microscope. We are also grateful to the members of the IOM-Leipzig for their support.

[1] K. Wien, Rad. Eff. Def. Sol. **109**, 137 (1989).

[2] I. A. Baranov, Y. M. Martynenko, S. O. Tsepelevich, and Y. N. Yavlinskii, Sov. Phys. Usp. **31**, 1015 (1988).

[3] I. A. Baranov, V. V. Obnorskii, and S. O. Tsepelevich, Nucl. Instrum. Methods Phys. Res., Sect. B **52**, 9 (1990).

[4] W. L. Brown, Mater. Res. Soc. Symp. Proc. **51**, 53 (1986).

[5] M. D. Hou, S. Klaumünzer, and G. Schumacher, Phys. Rev. B **41**, 1144 (1990).

[6] A. Audouard, E. Balanzat, J. C. Jousset, D. Lesueur, and L. Thomé, J. Phys. Condens. Matter **5**, 995 (1993).

[7] Details about the irradiation apparatus and the calculations of R_p can be found in Ref. [5].

[8] J. M. Robertson, M. Brouha, H. H. Stel, and A. J. C. van der Borst, in *Rapidly Quenched Metals,* edited by S. Steeb and H. Warlimont (North-Holland, Amsterdam, 1985), Vol. I, p. 79.

[9] G. Carter, M. J. Nobes, and J. L. Whitton, Appl. Phys. A **38**, 77 (1985); G. W. Lewis, M. J. Nobes, G. Carter, and J. L. Whitton, Nucl. Instrum. Methods **170**, 363 (1980).

[10] M. Fried, L. Pogány, A. Manuaba, F. Pászti, and C. Hajdu, Phys. Rev. B **41**, 3923 (1990); C. Hajdu, F. Pászti, M. Fried, and I. Lovas, Nucl. Instrum. Methods Phys. Res., Sect. B **19/20**, 607 (1987).

[11] A. Gutzmann, S. Klaumünzer, A. Benyagoub, and D. Nagengast, Rad. Eff. Def. Sol. **126**, 133 (1993); A. Gutzmann, Ph.D. thesis, Universität Leipzig, 1992 (unpublished).

[12] F. Garrido, Ph.D. thesis, Universtité Orsay, 1994 (unpublished)

[13] C. A. Volkert, J. Appl. Phys. **70**, 3521 (1991).

[14] C. A. Volkert and A. Polman, Mater. Res. Soc. Symp. Proc. **235**, 3 (1992).

[15] E. Snoeks, A. Polman, and C. A. Volkert, Appl. Phys. Lett. **65**, 2487 (1994).

[16] A. Barbú, M. Bimbole, R. Le Hazif, S. Bouffard, and J. C. Ramillon, J. Nucl. Mater. **165**, 217 (1989).

[17] Z. Zhu and P. Jung, Nucl. Instrum. Methods Phys. Res., Sect. B **91**, 269 (1994).

[18] S. Klaumünzer and A. Gutzmann (unpublished).

[19] S. Klaumünzer and A. Benyagoub, Phys. Rev. B **43**, 7502 (1991).

[20] In the most general case k_0 has to be replaced by a tensor of rank 4. In an amorphous material the tensor character can only result from polarization effects by the ion beam leading to three independent elements in the tensor. In this Letter these polarization effects are deliberately ignored.

[21] A_0 depends on S_e (see Refs. [5,6]) which depends on the penetration depths of the ions into the sample. R_p^* denotes the projected depth with $A_0[S_e(R_p^*)] \approx 0$. A more detailed analysis based on the results of Ref. [6] shows that $R_p^* = 10\ \mu$m is a good approximation for the ions of this particular experiment.

[22] R. G. Larson, Rheol. Acta **31**, 213 (1992).

[23] S. Klaumünzer, Ch. Li, S. Löffler, M. Rammensee, G. Schumacher, and H. Ch. Neitzert, Rad. Eff. Def. Sol. **108**, 131 (1989).

[24] H. Trinkaus and A. I. Ryazanov (to be published); H. Trinkaus, J. Nucl. Mater. (to be published).

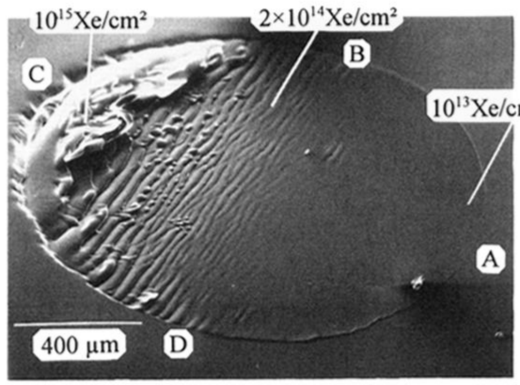

FIG. 2. This scanning electron micrograph illustrates the various stages of the surface modification during Xe implantation ($E = 2.64$ MeV/u, $T_i = 80$ K, $\theta = 45°$) into an originally polished sample. The fluence variation from the left to the right is also indicated. This sample was prepared only for illustration. The fluence values given in the text were derived from uniformly irradiated specimens. The coordinate system is x axis along line $CA \equiv$ the projection of the beam onto the plane surface, y axis along DB, z axis normal of the plane surface. The tilt angle θ is subtended by the beam axis and the z axis.